Petroleum Science 20 (2023) 2499–2511

Contents lists available at ScienceDirect

Petroleum Science

journal homepage: www.keaipublishing.com/en/journals/petroleum-science

Original Paper

Eco-friendly aqueous foam stabilized by cellulose microfibers with great salt tolerance and high temperature resistance

Li-Li Yang [a, *], Xian-Bo He [a], Yi-Xiu Cheng [b], Guan-Cheng Jiang [a, **], Ze-Yu Liu [a], Shi-Bo Wang [a], Shi-Xin Qiu [a], Jian-Hua Wang [c], Wei-Guo Tian [b, ***]

[a] MOE Key Laboratory of Petroleum Engineering, State Key Laboratory of Petroleum Resources and Engineering, China University of Petroleum (Beijing), Changping District, Beijing, 102249, China
[b] Beijing National Laboratory for Molecular Sciences, CAS Key Laboratory of Engineering Plastics, Institute of Chemistry Chinese Academy of Sciences (CAS), Haidian District, Beijing, 100190, China
[c] MOE Key CNPC Drilling Research Institute, Changping District, Beijing, 102206, China

ARTICLE INFO

Article history:
Received 25 November 2022
Received in revised form
3 February 2023
Accepted 15 May 2023
Available online 16 May 2023

Edited by Jia-Jia Fei

Keywords:
Aqueous foam
Foam stabilizer
Cellulose microfiber
Salt tolerance
Sustainable

ABSTRACT

A low-cost eco-friendly aqueous foam, especially the robust foam with great tolerance to high salinity and high temperature, is in great demand in the oil industry, e.g., oil and gas well or geothermal well drilling. Herein, an ultra-stable aqueous foam was developed using the biodegradable cellulose microfiber (CMF) as a foam stabilizer. The foam stabilized by CMF shows excellent tolerance to the high concentration of NaCl (6.0 wt%) and $CaCl_2$ (0.25 wt%) and the related drainage half-life times ($T_{0.5}$) reach 1750 and 2340 s respectively. By contrast, the foams without CMF are completely drained ($T_{0.5} = 0$ s) when NaCl concentration is greater than 6.0 wt% or $CaCl_2$ concentration is greater than 0.20 wt%. Notably, $T_{0.5}$ of the foams stabilized by CMF at these saline concentrations still can maintain above 1000 s even after aging at 120 °C for 16 h, exhibiting an outstanding foam-stabilizing performance at high temperature. Experimental results suggest that the salt and high-temperature tolerance of CMF in foam stabilization is attributed to the electrically uncharged surfaces, the formation of a gel-like structure and the excellent thermal stability. This work not only provides a promising candidate of aqueous foam stabilizer to deal with high temperature and high salinity but also presents a natural-based solution for an environmentally friendly drilling industry in the future.
© 2023 The Authors. Publishing services by Elsevier B.V. on behalf of KeAi Communications Co. Ltd. This is an open access article under the CC BY-NC-ND license (http://creativecommons.org/licenses/by-nc-nd/4.0/).

1. Introduction

The aqueous foam system is composed of a gas-liquid mixed phase. It has been widely used in various fields, such as food, cosmetics, ceramics, fire extinguishing, and pharmaceutical industries (Tang et al., 2020; Wang et al., 2017). Besides, aqueous foaming fluids have also been extensively applied in oil industries under harsh conditions, e.g. drilling, oil displacement, fracturing, geological carbon and hydrogen storage, acidification, and sand control, especially geothermal drilling and enhanced oil recovery (Majeed et al., 2019; Zhu et al., 2017; Chaturvedi et al., 2022; Sharma et al., 2022). Aqueous foam is inherently unstable from the perspective of thermodynamics and kinetics (Joshi, 2021). Due to the large specific surface area, the foam system has a high free energy, which leads to its thermodynamic instability and such instability is unavoidable (Rio and Biance, 2014). Kinetic instability factors include drainage, coalescence, and disproportionation. Drainage is a process in which the liquid in the liquid film is lost under pressure and gravity due to the extrusion of bubbles caused by surface pressure at the Plateau boundary (Conroy et al., 2013). Coalescence is caused by the collapse of the membrane between two adjacent bubbles, resulting in the fusion of two bubbles (Murray et al., 2006). Disproportionation, on the other hand, is the transfer of gas from small bubbles to large bubbles, causing the small bubbles to disappear (Briceno-Ahumada and Langevin, 2017). In fact, the three modes of foam instability can influence each other. For example, when two adjacent bubbles drain, the two bubbles will be close to each other and the surface will merge, leading to

* Corresponding author.
** Corresponding author.
*** Corresponding author.
E-mail addresses: yangll@cup.edu.cn (L.-L. Yang), 15600263100_1@163.com (G.-C. Jiang), wgtian@iccas.ac.cn (W.-G. Tian).

https://doi.org/10.1016/j.petsci.2023.05.007
1995-8226/© 2023 The Authors. Publishing services by Elsevier B.V. on behalf of KeAi Communications Co. Ltd. This is an open access article under the CC BY-NC-ND license (http://creativecommons.org/licenses/by-nc-nd/4.0/).

film rupture and coalescence. The merging of two bubbles can form a new large bubble, and the transfer of gas from the relatively small bubble to the newly merged large bubble can cause disproportionation (Fameau and Salonen, 2014). Of the three foam instability mechanisms, disproportionation behavior is the most difficult to mitigate, as even the most compact surfactant monolayer can only partially prevent gas from passing through (Disalvo, 1988).

Surfactants are the most frequently used foaming agents, due to their significant ability to decrease interfacial tension (Singh et al., 2021). However, the liquid drainage rate is very fast when only a surfactant is added. Singh et al. (2021) synthesized a bio-resource green surfactant (fenugreek seeds), and it showed good foaming and CO_2 foam stability up to 90 °C. According to previous studies (Wang et al., 2013; Emrani and Nasr-El-Din, 2017), the addition of polymer can play a good role in stabilizing bubbles. Water-soluble polymers, such as polyacrylamide, can improve foam stability by increasing the viscosity of base fluid (Pu et al., 2017; Narukulla et al., 2022). Pandey et al. (2021) explored the effect of temperature (30, 70, and 90 °C) on CO_2 foam prepared by a nonionic polymer (guar gum) and a surfactant (TX-100), and studied the influence of viscosity on the system performance, but did not cover the study under high temperature conditions. Various other foams have been made from the mixture solution of surfactants and polymers (Pandey et al., 2021; Sun et al., 2019). However, the thermal stability is far from satisfactory due to interaction variation and thermal degradation at high temperature.

The particles exhibit greater foam stabilizing ability because of the dramatically increased free energy of desorption. Therefore, the particles can accumulate and form a thick and mechanically robust layer at the interfaces between liquid and gas, and thus inhibit the coalescence of the bubbles (Qiao et al., 2020). Particle stabilizer has been widely studied and applied in the oil industry. Yang et al. (2019) previously made Janus silica nanoparticles and found that a commercial foaming agent can withstand temperature extremes of up to 280 °C using the Janus nanoparticles as a stabilizer. In another study, magnesium aluminum silicate nanosheets raised the temperature resistance up to 320 °C, showing much better foam stabilization ability of nanosheets compared to nanoparticles (Wang et al., 2020). In addition to the thermal stability, the stability of the foam in the presence of salts is also important since the formation water is saline.

Salt can inhibit the coalescence of bubbles above the transition concentration; thus affecting the stability and foamability of the foam. According to previous studies (Firouzi et al., 2015; Yaminsky et al., 2010), the effect of salt on foam stability depends on the concentration of surfactant in the system. When the surfactant dosage is below the critical micelle concentration, the addition of salt will promote foam stability because of the enhanced surfactant adsorption, while above the critical concentration, the increasing effect weakens and eventually remains the same or declined. The addition of salts has a similar influence on foamability. Foaming agents were usually added at concentrations above the critical concentration to prevent loss during circulation. In this case, foaming agents can be crippled when encountering high saline solution (Firouzi et al., 2015; Amani et al., 2021; Del Castillo et al., 2011). In surfactant-only foam systems, when there is no salt in the system, the foam liquid film is stabilized by electrostatic interaction, and the electrical double layer repulsive surface force plays the role of providing separation pressure, slowing down or preventing the water drainage of the liquid film, so that the foam remains stable. When a certain concentration of salt is added, the mutual adsorption of cations and surfactants at the air-water interface leads to a decrease in the mobility of the interface, and with increasing salt concentration, the migration rate becomes lower and lower, thus slowing the rate of diffusion and penetration of gases, so as to increase the stability of the foam (Craig, 2004). When the salt concentration exceeds the critical concentration, the excess salt reacts with the surfactant to form a precipitate, resulting in a significant decrease in the foaming and foam stabilization properties of the system (Zhang et al., 2017). We speculate that the effect of salt on foam stability can be mitigated by adding nano or micro materials as foam stabilizer.

According to Derjaguin-Landau-Verwey-Overbeek (DLVO) theory, colloidal stability of nano and micro-materials in water is related to electrostatic repulsion of surface charged functionalities and van der Waals attractive energy (Montes Ruiz-Cabello et al., 2013). The effect of salt on the stable bubble of nano particles or nano fluid can be attributed to the electrostatic action. For nanofluid foam stabilizer, high salt concentration will greatly reduce the repulsive force between nanoparticles, leading to serious agglomeration phenomenon, and then reduce the uniformity of nanoparticles on the foam liquid film, and eventually lead to worse bubble stabilization (Chaturvedi et al., 2021; Chaturvedi and Sharma, 2021). However, when surfactant is introduced into the system, the effect of salt on the stability of the foam system has not been clearly determined. What is clear is that, in some previous studies, the drainage half-life of foam systems decreases with increasing salt concentration, which is not beneficial for downhole applications. Janus particles/surfactant foam system and nano-magnesium aluminum silicate/surfactant system are two typical examples (Yang et al., 2019; Wang et al., 2020). Zwitterionic and neutral surfaces are less insensitive to electrolyte and their viscosity is increased with salinity, which can mitigate the foam destruction process. Therefore, the nano or micro-sized materials with previous characteristics might serve as an effective method. Especially, neutral surfaces absorb comparatively less foaming agent, which is beneficial to the foaming process. Besides, the current environmental issues and carbon peaking and carbon neutrality goals have led to new trends using eco-friendly, low-cost, and sustainable materials for the oil industry (Gupta, 2019). Therefore, the neutral nano or micro-materials made from natural polymers should be the appropriate candidates for aqueous foam stabilizer with adequate salt tolerance.

Cellulose is the most abundant natural polymer on earth and has been successfully transformed into diverse micro or nano-materials, such as cellulose micro/nanofibrils (CMFs/CNFs) and cellulose nanocrystals (CNCs), using TEMPO oxidation method. Xiang et al. (2019) confirm that CNF can improve the stability of anionic surfactant stabilized foam. Lv et al. (2021) have successfully applied CNF to foam stability, and studies have shown that the addition of CNF can effectively inhibit liquid film drainage and gas diffusion, so as to improve foam stability. Another study of CNF-stabilized water-based foam systems shows that the addition of NaCl and $CaCl_2$ can weaken the stability of the system because the carboxylated CNF interacts with salt ions to form aggregates (Ishii et al., 2022). It should be noted that CMF, CNF, and CNC from TEMPO oxidation method are too expensive for application in the oil industry. More importantly, the inherent charges on the surface of CMF, CNF, and CNC due to the introduction of carboxyl groups weaken their salt tolerance, resulting in poor downhole foaming stability.

Herein, we employed uncharged cellulose microfibrils (CMF) instead of charged cellulose nanocrystal as a foam stabilizer with excellent foaming stability, thermal stability, and salt tolerance. Foam stability after the addition of CMF and salts was thoroughly investigated to reveal the effect of micro-dimension and morphology of CMF on its foam stabilizing performance. The salt tolerance and high-temperature resistance of the CMF-stabilized foam were evaluated via the initial aqueous foam volume (V_0) and drainage half-life ($T_{0.5}$) of the CMF dispersion at different

concentrations of NaCl and $CaCl_2$. The experimental results showed great prospects for the use of CMF as a sustainable foam stabilizer in drilling field with harsh conditions, i.e., high salinity and high temperature. Additionally, since CMF is a wood-based material, it can be mass-produced, and due to its biodegradability (Klemm et al., 2005), it does not cause significant harm to the environment.

2. Experimental section

2.1. Materials

CMF which are microfibrils with a length of tens of micrometers and a diameter less than 3.0 μm were supplied by the Institute of Chemistry, Chinese Academy of Sciences. A commercial foaming agent AD300 was supplied by Dongying Aoda Petrochemical Co., Ltd. (China). Polyacrylamide (PAM), hydroxyethyl cellulose (HEC), hydrophilic nano silica (Nano-SiO_2) and other chemicals were of analytical grade and purchased from Beijing Inokai Technology Co., Ltd (China). All chemicals were directly used as received.

2.2. Characterization of CMF

The CMF was dispersed into deionized (DI) water with a vigorous stirring for 30 min to prepare 0.01 wt% CMF dispersion. The microstructure of the dispersed CMF was observed under an optical microscope (DM4M, Leica, Germany). The micromorphology of the dried CMF was performed using a scanning electronic microscope (SEM, SU8010, Hitachi, Japan). CMF dispersion was dropped on a holder and dried at 60 °C prior to measurement.

The thermal stability of CMF was determined by thermogravimetric analysis (TGA, Pyris-1, PE, USA) at a heating rate of 10 °C·min^{-1} and under N_2 flow.

The chemical structure of CMF was confirmed through a Fourier transform infrared spectrometer (FTIR, Magna-IR 560, Nicolet, USA) in the wavenumber range of 4000–400 cm^{-1} and at a resolution of 4 cm^{-1}.

The interlayer distance of CMF was determined by X-ray diffraction (XRD) measurements (Rigaku, Japan) with Cu target (λ = 1.5406 Å). CMF was measured in the range of 5–25° at a scanning rate of 0.5°·min^{-1}. The basal spacing was analyzed according to Bragg's equation.

The Zeta potential of CMF dispersion was determined using a nanoparticle size and Zeta potential analyzer (SZ-100, Horiba, Japan). The concentration of CMF dispersion was 0.1 wt%.

2.3. Preparation of CMF/AD300 mixture dispersions

A total of 100 mL of CMF dispersions (1.0 wt%) was prepared by mechanical stirring at 1000 rpm for 30 min. Then, 0.4 wt% AD300 was added to each dispersion and stirred at 1000 rpm for an additional 10 min. Hereafter, NaCl (1.0–7.0 wt%) or $CaCl_2$ (0.05–0.3 wt%) was added into the CMF/AD300 mixture dispersions to evaluate the monovalent and divalent salt tolerance of foam, respectively.

The behavior of dispersion after aging at high temperature was then tested. In detail, 350 mL dispersions of the CMF/AD300 mixture were prepared and transferred into aging tanks (Tongchun, China), followed by hot rolling at 120 °C for 16 h in a roller oven (Tongchun, China). After the temperature was cooled down to room temperature, the thermally aged dispersions were obtained.

2.4. Performance of CMF on foaming ability and foam stabilization

Foamability and foam stabilization were tested using a modified Waring blender method. A total of 100 mL of dispersion was vigorously stirred at 11,000 rpm for 1.0 min. After stirring, the well-prepared foams were promptly transferred into a measuring cylinder. Then V_0 and $T_{0.5}$ were recorded to evaluate the foamability and foam stability, respectively. V_0 is the initial foam volume; while $T_{0.5}$ is the time required for the foam to drain 50% of the original liquid volume.

A portion of the as-prepared foam was placed on a slide and gently covered with a coverslip. The morphology of the bubbles over time was observed with the optical microscope mentioned above. Film thickness and bubble diameter were obtained by analyzing the micrographs through ImageJ software.

Cryo-SEM imaging was performed on an FEI Helios NanoLab G3 CX Emission SEM (USA) equipped with a Quaroum PP3000T low-temperature sample holder, to examine foam morphology. The samples were loaded on the cryo-specimen holder and cryo-fixed in liquid nitrogen, then quickly transferred to the cryo-stage (Quorum Technologies, PP300T, East Sussex, UK), a chamber attached to the microscope. Once the sample was inside the chamber, the sample was fractured to obtain cryosections for examination. The surface was then coated with wolfram (10 mA, 30 s) and then transferred to the microscope chamber where it was analyzed at a temperature of −180 °C.

2.5. Rheological properties measurements

The rheological properties of different dispersions were determined by a ZNN-D6L rotational viscometer (Tongchun, China), and operated at the rates of 600 and 300 rpm. The apparent viscosity (AV) and plastic viscosity (PV) were calculated according to the following equations:

$$AV = \theta_{600}/2 \tag{1}$$

$$PV = \theta_{600} - \theta_{300} \tag{2}$$

where θ_{600}, and θ_{300} are the readings at 600 and 300 rpm, respectively.

The elastic modulus (G') of the dispersions was tested using the lamina module of the rheometer (Haake MARS 60, Thermo Fisher Scientific, USA). The conical rotor model was C35 1°/Ti (the cone angle of the rotor was 1° and the diameter was 35 mm), and the gap between the rotor and the sample stage was 0.053 mm during the test. The strain scan was performed with a fixed frequency of 1 Hz and in a strain range of 0.01%–1.0%. A strain of 0.1% was selected during the frequency sweep, the suspension was in the linear viscoelastic region at this time, and the frequency range was 0.1–10 Hz. To eliminate shear interferences when loading samples, each sample was pre-sheared (3 min at 1000 s^{-1}) before the start of each measurement, and rested for 5 min before the following tests.

The surface tension and the interfacial dilatational modulus of different dispersions of CMF/AD300 mixture were measured by a tensiometer (Tracker-H, Teclis, France) at a sinusoidal oscillation frequency of 0.1 Hz.

3. Results and discussion

3.1. Fundamental properties of the foam stabilizer CMF

Cellulose is the most abundant natural polymer on earth. It is an amphiphilic polysaccharide that hierarchically self-assembles into fibers. Therefore, cellulose is a perfect low-cost and sustainable raw material to make up micro, nano-fibers for oilfield applications (Alqus et al., 2015; Medronho et al., 2012; Yokota et al., 2021). As depicted in Fig. 1(a), the uncharged CMF was obtained from the wood pulp to stabilize the aqueous foam for the hydrothermal well

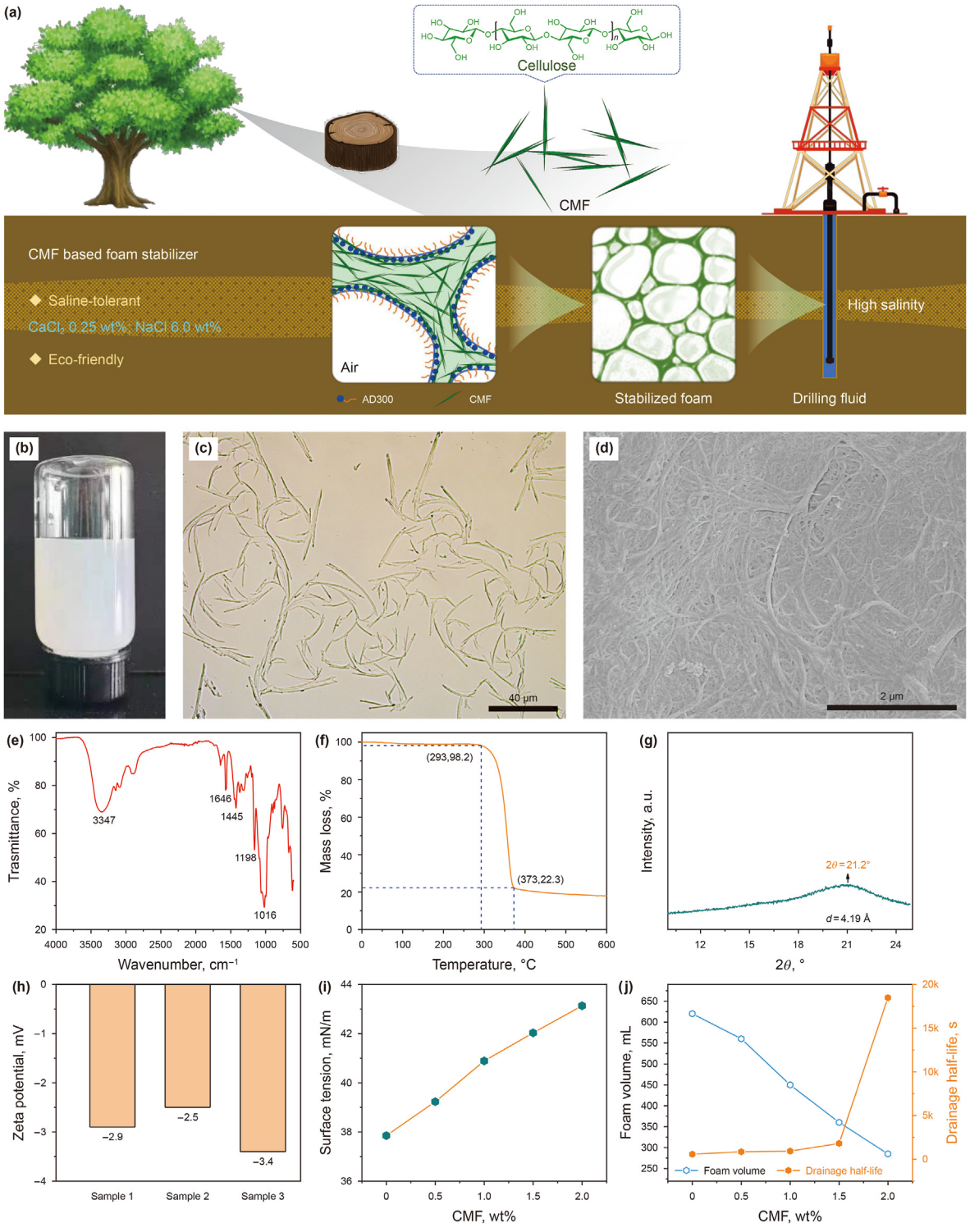

Fig. 1. Fundamental properties of CMF for foam stabilization. (**a**) Origin of CMF for foam stabilization in schematic illustration. (**b**–**c**) Digital and microscopic photographs of CMF in aqueous suspension. (**d**) SEM image of the dry CMF. (**e**–**g**) FTIR, TGA, and XRD analysis of CMF. (**h**) Zeta potential of CMF in aqueous suspension. (**i**) Surface tension of CMF/AD300 mixtures at different concentrations of CMF (wt%), respectively. (**j**) Foam volume (V_0) and drainage half-life ($T_{0.5}$) of the foam stabilized with CMF at different concentrations (wt%).

drilling under harsh circumstances (high temperature and high salinity). Fig. 1(b) also shows that CMF is a stable opalescent dispersion with regular morphologies and relatively uniform size in water. In detail, these are microfibrils with a length of tens of micrometers and a diameter less than 3 μm (Fig. 1(c)), corresponding to an aspect ratio between 10 and 100. The relatively large specific surface area ensures complete hydration and stable dispersion of CMF in water. The SEM image in Fig. 1(d) shows that the dried CMF self-assembled a smooth and flat membrane. Fig. 1(e) shows the typical FTIR spectrum of CMF (3347 cm^{-1}, —OH, stretching vibration; 1646 cm^{-1}, O—H, bending vibration; 1445 cm^{-1}, C—H, bending vibration; 1315 cm^{-1}, —O—H, bending vibration; 1198 cm^{-1} and

1016 cm^{-1}, –C–O, stretching vibration).

The XRD patterns of CMF are illustrated in Fig. 1(g). The broad and flat peak around 22° indicates that the crystalline degree of CMF was decreasing compared to natural cellulose (Chen, 2014). This result demonstrates the successful manufacture of CMF.

The TGA result in Fig. 1(f) demonstrates that CMF is thermally stable below 293.0 °C. When the temperature is raised from 293 to 373 °C gradually, the weight of CMF drops from 98.2% to 22.3%. However, up to 600 °C, 17.98% remained. The TGA measurement reveals that the CMF possesses great thermal stability to withstand the high downhole temperature.

The Zeta potential measurements (Fig. 1(h)) of CMF are as followed: −2.9, −2.5, and −3.4 mV, and the average value is about −2.93 mV. According to previous research, the potential of cellulose nanocrystal (CNC) from TEMPO oxidation is generally about −37 mV (Banerjee et al., 2020). In contrast, the surface potential of CMF is negligible.

3.2. Foam stabilization performance of CMF

The foaming agent, AD300, is high temperature resistant and is used to evaluate the foam stabilization performance of CMF. The critical micellar concentration (CMC) of AD300 is 0.35 wt%. Fig. 1(i) shows that the surface tension of CMF/AD300 dispersion increases with increasing CMF concentration (0–2.0 wt%). When the concentration of foaming agent is higher than 0.35 wt%, colloidal aggregates are produced (Bąkowska et al., 2022; Novev et al., 2017; Chaiyasit et al., 2007), but in the dispersion of the CMF/AD300 mixture, a small amount of AD300 is adsorbed on the surface of CMF, which leads to a slight increase in CMC. It is precisely because of the adsorption phenomenon that the dosage of AD300 in the system must be set slightly higher than 0.35 wt% to ensure a stable foam system. Therefore, we determine that the concentration of AD300 is 0.40 wt%.

Fig. 1(j) illustrates that V_0 and $T_{0.5}$ without salt are functions of CMF concentration. With increasing CMF concentration, V_0 shows a gradually decreasing trend. In detail, V_0 decreases from 620 to 285 mL with the increase from 0 to 2.0 wt% of CMF. Regarding foam stabilization performance, $T_{0.5}$ displays a positive correlation with CMF concentration, and it significantly increases from 566 to 18,480 s, about 32.6 times in the same concentration range of CMF. To ensure sufficient foaming ability, in the following study, 1.0 wt% of CMF is added if no special statement is given. In this case, V_0 reaches 450 mL and $T_{0.5}$ is as high as 924 s. Compared to the AD300 solution, the $T_{0.5}$ of the dispersion of CMF/AD300 mixture is increased by 1.6 times.

In order to demonstrate the benefits of CMF in foam stability and salt tolerance, a series of controlled experiments are conducted. Three commonly used foam stabilizers including PAM, HEC, and Nano-SiO_2 are selected. Their foam stabilities at ambient temperature are explored and compared with CMF. Their concentrations are determined according to their viscosities. PAM and HEC are of high viscosity due to the high molecular weight, and the concentration is 0.1 wt%; while Nano-SiO_2 has similar viscosity with CMF and the concentration is 1.0 wt%. As shown in Fig. 2(a) and (b), the foaming volume of the PAM stabilized foam system is much smaller than that of the other three foam stabilizing agents, and the foaming volume shows a decreased tendency with increasing NaCl or $CaCl_2$ dosage. When the NaCl dosage is 6.0 wt%, the foaming volume is reduced to only 150 mL. Therefore, PAM exhibits a severe impact on the foaming ability, while the foamability of CMF, HEC and Nano-SiO_2 has no big difference. Regarding the foam stabilizing effect (Fig. 2(c) and (d)), the system containing PAM shows the longest drainage half-life, and increases with the dosage of NaCl or $CaCl_2$. The drainage half-life of the system containing Nano-SiO_2 is shorter at all salinities. HEC and CMF have better foam stabilizing performance; it is because of the amphiphilic property of cellulose-based materials. At low dosage of NaCl or $CaCl_2$, the drainage half-life of the system with HEC is slightly higher than that of CMF containing system. With increasing the concentration of NaCl or $CaCl_2$, the drainage half-life of CMF containing system gradually exceeds that of HEC. It indicates that the addition of CMF is conductive to enhancing the foaming and foam stabilization performance in presence of salt simultaneously. The temperature resistance comparison between CMF and HEC is performed at 120 °C (Fig. 2(e)–(h)). At low salt concentration, the foaming volume of HEC foam system is higher than that of CMF foam system, but with the increase of NaCl or $CaCl_2$, the latter exceeds. From the perspective of drainage half-life, the drainage half-life of CMF foam system increases with increase in NaCl or $CaCl_2$ concentration, while the drainage half-life of HEC foam system exhibits a decrease trend and the drainage half-life of the former is always greater than that of the latter. At 120 °C, the foam system stabilized by CMF has better stability.

3.3. Salt tolerance of the foam stabilized by CMF

To simulate saline formation water, the dispersion of the CMF/AD300 mixture is contaminated with NaCl or $CaCl_2$ with varying concentrations before measurements. It is observed that V_0 shows a decreasing trend with increase in the concentration of NaCl or $CaCl_2$ (Fig. 3(a) and (d)). When NaCl is less than 6.0 wt%, V_0 decreases slightly, and the total volume reduces merely by 50 mL compared to that without NaCl. However, when the concentration of NaCl is continuously increased from 6.0 to 7.0 wt%, V_0 drops dramatically from 400 to 355 mL. The influence of $CaCl_2$ on the foam stability is similar to NaCl. It has a moderately negative impact on V_0 when $CaCl_2$ concentration is less than 0.25 wt%, while V_0 strongly decreases when the concentration is above 0.25 wt%. Comparatively, $CaCl_2$ has a greater impact on foaming ability than NaCl. The effect of saline concentration on $T_{0.5}$ is also assessed. As shown in Fig. 3(c) and (f), $T_{0.5}$ shows a monotonically increasing trend with increasing NaCl concentration. Specifically, when the NaCl concentration increases from 0 to 7.0 wt%, $T_{0.5}$ is extended from 924 to 1921 s. When the concentration of $CaCl_2$ increases from 0 to 0.3 wt%, a turning point of $T_{0.5}$ showed at 0.25 wt% of $CaCl_2$ instead of a monotonic trend. However, when the concentration of $CaCl_2$ increases from 0 to 0.25 wt%, $T_{0.5}$ extends from 924 s to the maximum value of 2340 s, continuing to increase the $CaCl_2$ concentration to 0.3 wt%, $T_{0.5}$ shows an obvious decrease from 2340 to 1990 s. The effect of salt on foam stability has been studied experimentally and theoretically. The effect of salt on foam system is twofold (Firouzi et al., 2015; Yaminsky et al., 2010). Below the critical value, the increase of salt concentration will promote the stability of the foam system, and beyond the critical value, the stability of the foam system will gradually weaken. This also explains the turning point in the drainage half-life curve shown above. In a study of CNF-stabilized water-based foam by Ishii et al. (2022), the addition of salt can increase the adsorption capacity of negatively charged CNF at the air/liquid interface, thus increasing the viscoelastic modulus, which will promote the foam to be more stable. When the salt concentration exceeds a certain value, excessive cations (Na^+, Ca^{2+}) easily leads to the formation of unevenly dispersed CNF aggregations, which reduces the stability of foam. In the study, salt ions affect the distribution of CNF mainly through electrostatic interactions. By contrast, in our study, CMF is almost electrically neutral, and the electrostatic interactions are much weaker. Based on this, it is necessary to deeply explore the effect of salt on CMF.

Two main reasons affect the stability of the foam, namely the drainage of the bubbled liquid film and the diffusion of the gas

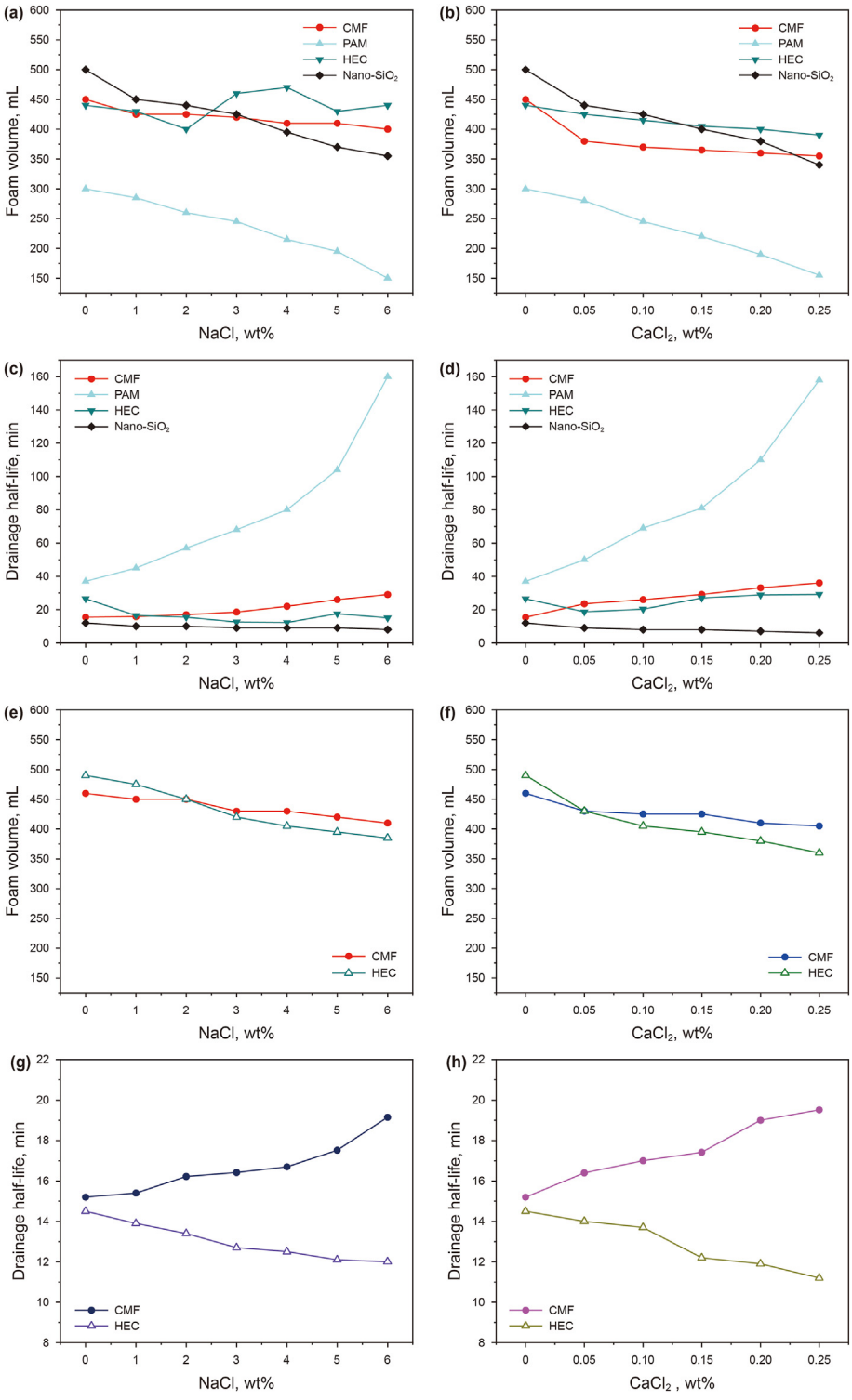

Fig. 2. Foam volume of the foam stabilized by CMF, PAM, HEC and Nano-SiO_2 at (**a**) different NaCl concentrations and (**b**) different $CaCl_2$ concentrations at ambient temperature; drainage half-life of the foam stabilized by CMF, PAM, HEC and Nano-SiO_2 at (**c**) different NaCl concentrations and (**d**) different $CaCl_2$ concentrations at ambient temperature. Foam volume of the foam stabilized by CMF and HEC at (**e**) different NaCl concentrations and (**f**) different $CaCl_2$ concentrations after aging at 120 °C; drainage half-life of the foam stabilized by CMF and HEC at (**g**) different NaCl concentrations and (**h**) different $CaCl_2$ concentrations after aging at 120 °C.

phase through the liquid film. Drainage of the bubbled liquid film occurs when the surface pressure from the plateau boundary forces bubbles to squeeze each other, leading to the loss of the liquid from the bubble films under pressure and gravity. As a result, the bubble films become thinner and thinner until the bubbles burst. The diffusion of the gas phase across the liquid film is divided into two cases: for the bubbles at the edge of foam, the gas directly bursts into air and for the bubbles inside the foam, the gas in the small bubbles diffuses towards larger bubbles because smaller bubbles generally have higher internal pressure. Then the small bubbles

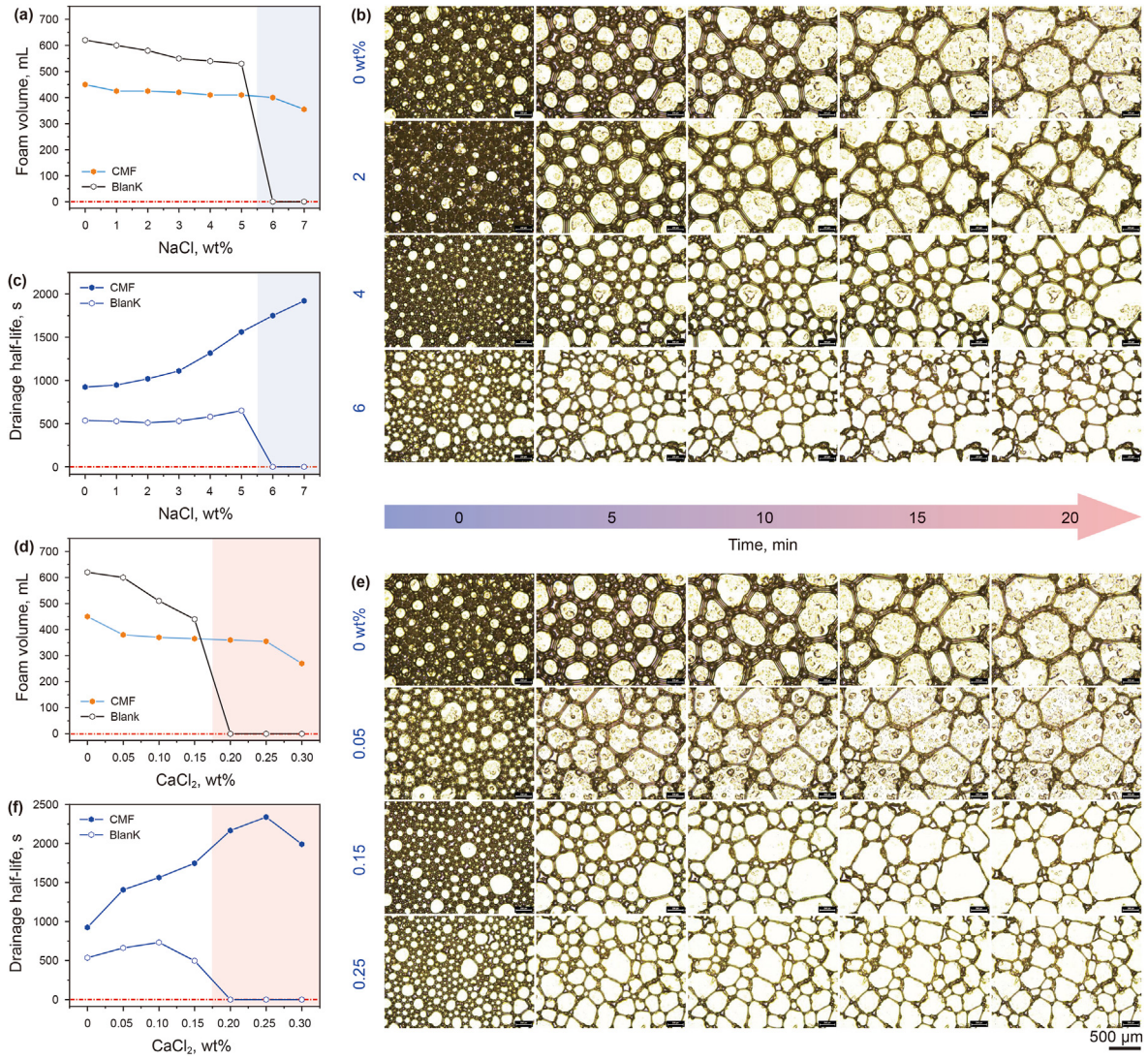

Fig. 3. Salt tolerance of the foam stabilized by CMF. (**a**) Foam volume (V_0), (**b**) microscope images at different time, and (**c**) drainage half-life ($T_{0.5}$) of the foam stabilized by CMF at different concentrations of NaCl (wt%). (**d**) Foam volume (V_0), (**e**) microscope images at different time, and (**f**) drainage half-life ($T_{0.5}$) of the foam stabilized by CMF at different concentrations of $CaCl_2$ (wt%).

disappear and the foam volume decreases. As depicted in Fig. 3(b) and (e), the foam undergoes disproportionation and coalescence over time. The bubbles in the foam with NaCl and $CaCl_2$ are richer and delicate in comparison with the control group. It is observed that the bubbles in the control group disproportionate and coalesce very quickly. After 5.0 min, the number of small bubbles is greatly reduced, while the number of large bubbles increases significantly. After 15.0 min, small bubbles almost disappear. On the other hand, for foams with NaCl and $CaCl_2$, the rate of disproportionation and coalescence is slowed down. Only a few large bubbles exist after 5.0 min, and there are still a large number of small bubbles after 15.0 min. As the concentration of NaCl and $CaCl_2$ is increased, the foam stability is further improved.

3.4. High-temperature (120 °C) tolerance of the foam stabilized by CMF

The foam stability of the dispersion of CMF/AD300 mixture is further evaluated after being aged at 120 °C. As illustrated in Fig. 4(a) and (b), the foam volume, V_0 shows a decreasing trend with increasing NaCl or $CaCl_2$ concentration, exhibiting remarkable similarities with before aging. Additionally, V_0 increases slightly at each salinity compared with those before aging. As shown in Fig. 4(c) and (d), $T_{0.5}$ still increases with the increase in NaCl and $CaCl_2$ concentrations. When the concentration of NaCl increases from 0 to 6.0 wt%, $T_{0.5}$ increases from 912 to 1149 s, with an increase of 1.25 times. When the concentration of $CaCl_2$ increases from 0 to 0.25 wt%, $T_{0.5}$ increases from 912 to 1171 s, with an increase of 1.28 times. Compared with before aging, $T_{0.5}$ is decreased. Also, the increase of $T_{0.5}$ decreases with the increase of NaCl and $CaCl_2$ concentrations. Liquid phase viscosity is one of the factors affecting foaming ability and foam stability. The decreases viscosity due to thermal treatment results in the dispersion, exhibiting better foaming properties and relatively poor foam stabilization after aging, which will be elaborated in the following part.

3.5. Foam-stabilizing mechanism study of CMF

3.5.1. Surface tension

According to the Gibbs principle, the system always tends to adopt a lower surface energy mode. Low surface tension results in low surface energy, thus generating a stable multi-phase system

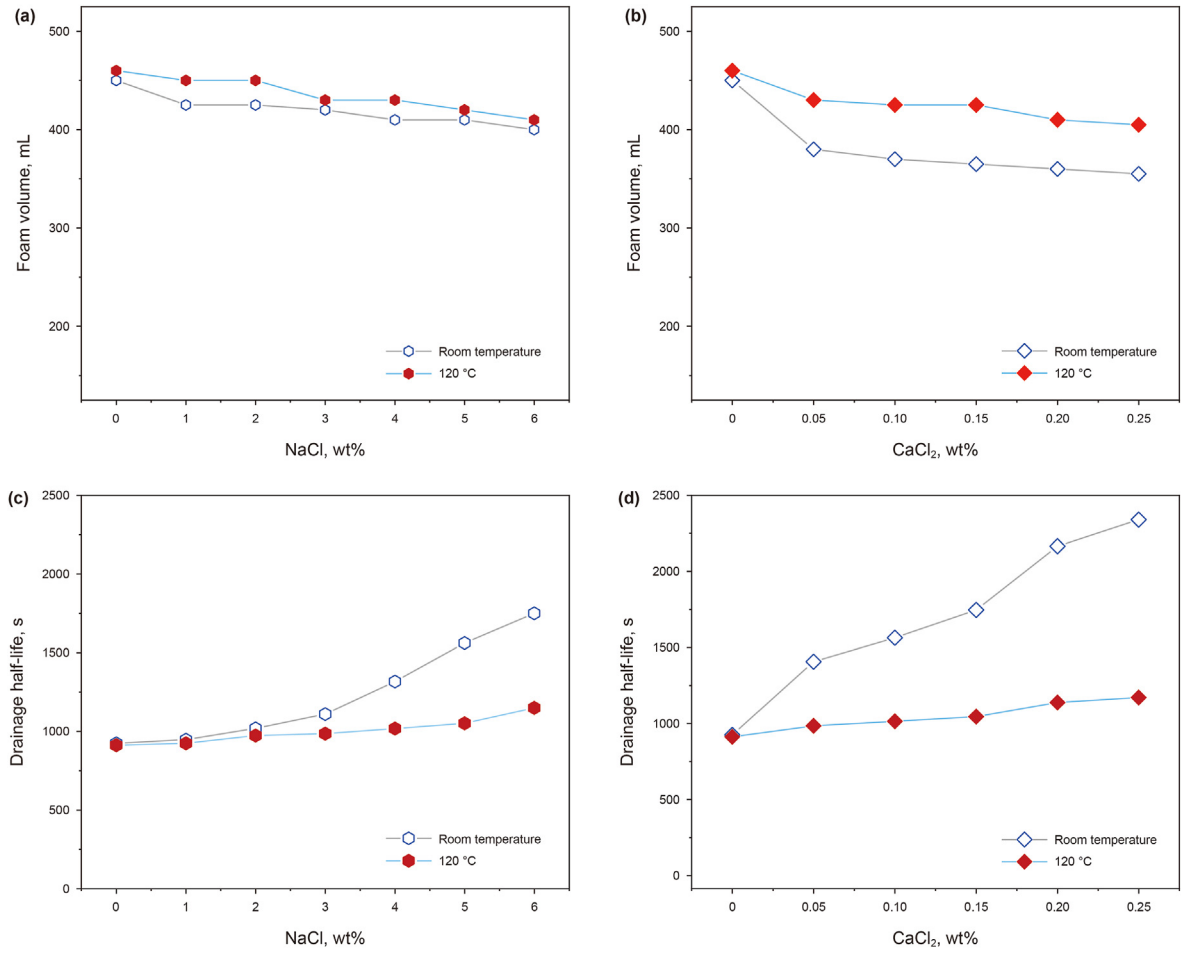

Fig. 4. High-temperature (120 °C) tolerance of the foam stabilized by CMF. (**a**) Foam volume (V_0) and (**c**) drainage half-life ($T_{0.5}$) of the foam stabilized by CMF at different concentrations of NaCl (wt%) after aging at 120 °C. (**b**) Foam volume (V_0) and (**d**) drainage half-life ($T_{0.5}$) of the foam stabilized by CMF at different concentrations of $CaCl_2$ (wt%) after aging at 120 °C.

(Wang et al., 2016). As depicted in Fig. 5(a) and (b), the addition NaCl and $CaCl_2$ decreases the surface tension, consistent with that reported in the literatures. However, the foaming ability is reduced with increasing salt concentration, although the reduction of surface tension is favorable to make up foam and producing a larger foam volume theoretically. It is speculated that salt interacts with AD300 and CMF, which impedes the foaming process. Unlike the foaming ability, the foam stability is enhanced as NaCl and $CaCl_2$ concentrations increased. This can be explained mainly by the fact that the reduction in the volume of foam results in a decrease in the volume percentage of the air phase, thus corresponding to a better stability of the foam. Reduction of foam volume and surface tension are not sufficient conditions for improving foam stability. Abascal and Gracia-Fadrique (2009) studied the surface tension and foam stability of commercial calcium and sodium caseinates. Although CaCN and NaCN has similar surface tension and critical concentration, However, the foam stability of NaCN is better than that of CaCN, because it takes longer time for CaCN to reach equilibrium at critical concentration and the molecular surface area is larger. The foam stability is also poor when the foam volume is reduced due to incomplete foaming. Therefore, it deserves to shed deep light on the stabilizing mechanism of foam.

3.5.2. Interfacial dilational modulus

In our study, the foam includes gas, liquid and solids, and the stability of the foam mainly depends on the stability of the liquid film, which can be well characterized by the interfacial dilational modulus. The resistance and self-repair ability of the liquid film are positively correlated with the interfacial dilational modulus. The larger the interfacial dilational modulus is, the stronger the resistance and self-repair ability of the liquid film will be (Yao et al., 2018; Xie et al., 2019). As shown in Fig. 5(c) and (d), all interfacial dilational modulus are unchanged over time. The interfacial dilational modulus of the dispersion of the CMF/AD300 mixture is about 1.0 $mN \cdot m^{-1}$. With the addition of NaCl and $CaCl_2$, the interfacial dilational modulus increase. When NaCl is added at a concentration of 6.0 wt%, the interfacial dilational modulus increases to approximately 4 $mN \cdot m^{-1}$. The as-prepared foam displays the longest $T_{0.5}$. Similar to NaCl, the interfacial dilational modulus increases to a maximum value when the concentration of $CaCl_2$ is increased to 0.25 wt%.

A foam with a high interfacial dilational modulus can prevent drainage, Ostwald ripening and bubble coalescence in the foam, thus exhibiting better stability. However, according to the Gibbs stability criterion $E > \gamma/2$, where E is the dilational elasticity ($mN \cdot m^{-1}$), and γ is the surface tension ($mN \cdot m^{-1}$) (Yao et al., 2018), the foam in our study is unstable from the energy point of view since the interfacial dilational modulus is well below half its surface tension. As for the saline/CMF solutions with the same interfacial dilational modulus when adding each of them at a certain concentration $CaCl_2$ series display stronger foam stabilization capacity than NaCl series, taking 0.05 wt% $CaCl_2$ and 2.0 wt% NaCl as an

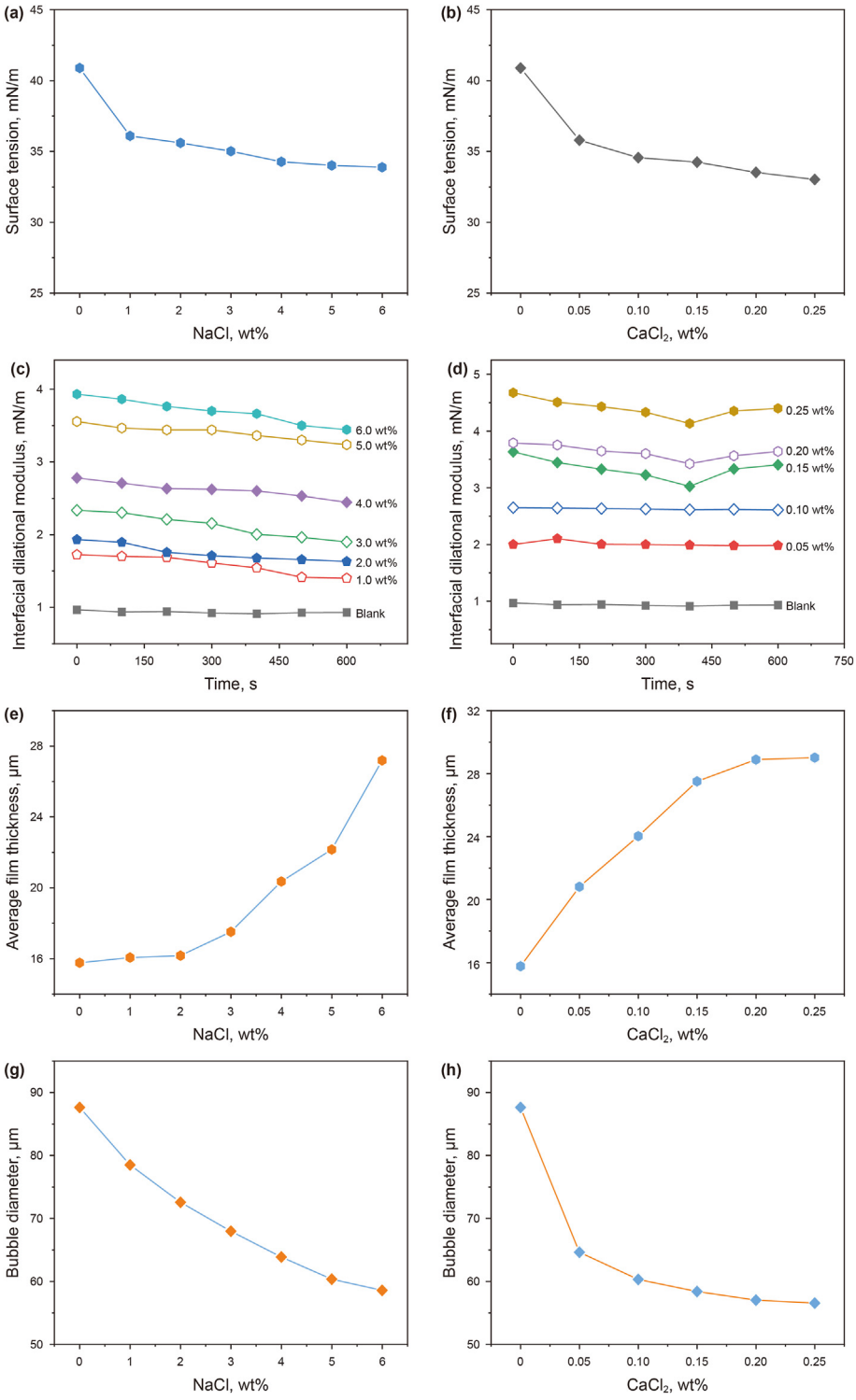

Fig. 5. Fundamental properties of the foam stabilized by CMF. (**a**) (**b**) Surface tension, (**c**) (**d**) interfacial dilational modulus, (**e**) (**f**) bubble film thickness, and (**g**) (**h**) bubble diameter of the foam at different concentrations of NaCl and $CaCl_2$ (wt%). The concentration of CMF was 1.0 wt%.

example. The foam system that follows the Gibbs stability criterion is stable, but this criterion obviously has its applicable scope. The CMF foam system in this study can still maintain good stability even if it does not meet this criterion. This system has been found in other studies (Wang et al., 2020). In order to more accurately explain the bubble stabilization mechanism of CMF, other properties of the bulk need to be further tested. According to existing studies (Wang et al., 2019; Czakaj et al., 2020), nanocellulose will be gelation under the action of salt, which will increase the viscoelastic modulus of the system and make the foam more stable. Based on this, it is necessary to further study the rheology of CMF system.

3.5.3. Bubble film thickness and diameter

The thickness of the liquid film and the bubble diameter are the basic properties of the foam. From Fig. 5(e)–(h), as the concentration of NaCl and $CaCl_2$ increasing, the average liquid film thickness of the bubbles increase, while the average diameter of the bubbles decreases. It is in accord with the foam stability performance and the interfacial dilational modulus results. The increase in viscosity may hinder the penetration of gas into the dispersion and migration of surfactant molecules from the dispersion to the air/liquid interface, thus resulting in a decrease in the initial foam volume and simultaneously in the diameter of the bubbles, and the thickness of the foam film has been increased during the foaming process. CMF is entangled with each other and can form a network structure. With the addition of salt, NaCl and $CaCl_2$ dissolved in water can form hydrated Na^+, hydrated Ca^{2+} and hydrated Cl^- (Briscoe et al., 2000). They break the hydrogen bonds between CMFs and form hydrogen bonds with the hydroxyl groups on the surface of CMF. Through hydrogen bonds between ionized water molecules and hydroxyl groups on the surface of CMF, CMF accumulates more at the air/liquid interface, which increases the thickness of liquid film. With the addition of salt, the thickness of foam film increases, therefore the foam stability improves. The increased stability improves the ability of the system to prevent bubble coalescence, hence the average bubble size observed is smaller.

3.5.4. Rheological properties of dispersions

As shown in Fig. 6(a) and (c), the presence of NaCl or $CaCl_2$ increases the AV of the dispersion. Increasing AV impedes the migration of molecular surfactants to the air/liquid interface and reduces the foaming efficiency and results in decreased foam volume. While higher dispersion viscosity delays the drainage process of the liquid film and slowing the rate of the film thinning, which promote the increase of foam stability (Said et al., 2022; Wei et al., 2022). However, AV no longer increases when more NaCl and $CaCl_2$ are added, but the foam volume and stability substantially decreases and increases, respectively. After aging, AV of all solutions drops evidently, but it remains insensitive to salt concentration as before aging (Fig. 6(b) and (d)). AV is composed of the friction between particles, solvent, polymers, and surfactants and the strength of the network structure. Although AV no longer changes as the salt concentration increases, the structure is literally enhanced according to the elastic modulus results (Fig. 6(e) and (f)), which in turn increases the structural strength and improves foam stability. Furthermore, the G' discrepancy between NaCl and $CaCl_2$ series is consistent with the foam stability results. Therefore, the rheological property, especially the strength of the network structure, contributes a lot to the stability of the foam as the salinity increases.

The effects of salt on the rheological properties the CMF dispersion are multiple, among which the CMF-solvent interaction and the electrostatic interaction between CMF and ions are most important (Xiao and Frey, 2008). It is reported that cations, couple to the same anion counterpart, Cl^- in this case, affect the gelatinization process in the following order $Mg^{2+} > Ca^{2+} > Li^+ > Na^+ > K^+$ (Viturawong et al., 2008). It is reported that carboxylated CNF is stably dispersed at NaCl concentrations of $\leq$ 50 mM and loses its fluidity and partial gelation took place at NaCl concentrations of $\geq$ 100 mM (Liu et al., 2018), and this can be attributed to the electrostatic interaction between Na^+ and COO^-. In this study, the G' of CMF foam system is increased as the salt concentration increased. However, in contrast to carboxylated CNF, CMF has almost no charge, and its very weak electrostatic interaction with salt ions is clearly not the cause of the increase in G'. With the addition of salt, NaCl and $CaCl_2$ dissolved in water can form hydrated Na^+, hydrated Ca^{2+} and hydrated Cl^- (Briscoe et al., 2000). They break the hydrogen bonds between CMFs and form hydrogen bonds with the hydroxyl groups on the surface of CMF. Through hydrogen bonds between ionized water molecules and hydroxyl groups on the surface of CMF, CMF accumulates more at the air/liquid interface. This phenomenon can explain that G' of CMF foam system increases with the increase of salt concentration. Therefore, the gel-like network structure of CMF is enhanced with the increase of salt concentration.

3.5.5. Micromorphology analysis of the foam stabilized by CMF

Encouraged by the above results, foams were observed by cryo-SEM observation. As shown in Fig. 7(a) and (d), CMF exists at the air/liquid interface, and the majority is in aqueous phase. The CMF self-assembled in the aqueous phase in the absence of salt. The remarkable similarities in parallel distribute direction in aqueous phase and bubble surface are also found. Salt can promote the formation of dense networks of CMF. Foam stabilized by CMF/NaCl exhibits mostly regular aligned distribution (Fig. 7(b) and (e)), while foam stabilized by CMF/$CaCl_2$ has larger network density (Fig. 7(c) and (f)), suggesting that CMF/salt interaction is very important for foam stability. It has also been shown that the bubble surface becomes flat and smooth. The adsorption of CMF at the air/liquid interface can explain the liquid film's better elastic properties and the increase in AV, especially the interfacial dilational modulus of the liquid film. As a result, the stability of the foam is significantly improved.

3.5.6. Proposed mechanism of CMF to stabilize foam at high temperature and high concentration of NaCl and $CaCl_2$

CMF can form a gel-like network at the air/liquid interface by interaction, which hinders the gas from entering the base liquid and prevents the migration of surfactant molecules from the water phase to the air/liquid interface. Consequently, the stability of the foam is improved. The addition of salt can make CMF networks denser and stronger, improve the interfacial dilational modulus of the liquid film, and play a positive role in increasing the thickness of the foam liquid film and reducing the size of the bubbles. Thus, CMF can significantly extend the drainage half-life and enhance the salt tolerance of the foam. Additionally, due to the excellent thermal stability, CMF networks can keep the structure integrity at the air/liquid interfaces under 120 °C for a long time. Accordingly, the foam also has a high resistance to high temperatures.

4. Conclusion

(1) CMF is used as an eco-friendly salt resistant foam stabilizer. Compared to other common molecule foam stabilizers, CMF can maintain excellent foam stability in the presence of NaCl and $CaCl_2$ up to 6.0 wt% and 0.25 wt%, respectively.

(2) CMF mainly adsorb on the bubble liquid film to achieve foam stabilization effect. They can improve the interfacial dilational modulus of the liquid film and enhance the salt tolerance of the aqueous foam.

(3) The addition of NaCl or $CaCl_2$ can promote the formation of gel-like network structure of CMF and increase the viscoelastic modulus of the liquid phase, thereby increasing the strength of the gel-like network structure, so as to build a more stable foam system.

(4) CMF has good thermal stability. We confirm that after aging at 120 °C, there will be no obvious negative impact on the formation of gel-like network structure of CMF. Therefore, the CMF foam system has a high temperature resistance of 120 °C.

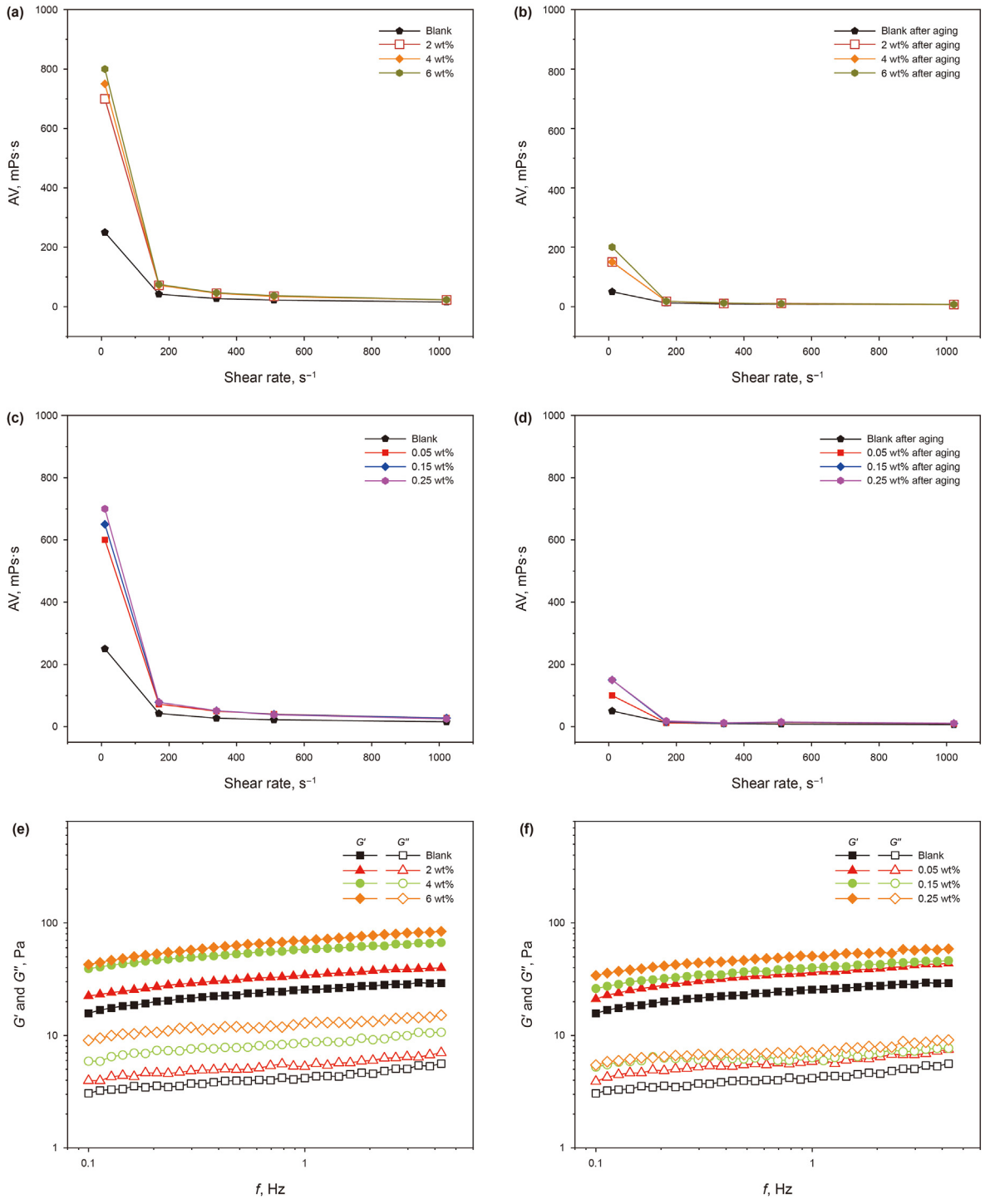

Fig. 6. Rheological properties of dispersions. (**a**) (**c**) Apparent viscosity (AV) and (**e**) (**f**) elastic modulus (G') and viscous modulus (G'') of dispersions at different concentrations of NaCl and $CaCl_2$ (wt%). (**b**) (**d**) Apparent viscosity (AV) of dispersions at different concentrations of NaCl and $CaCl_2$ (wt%) after aging at 120 °C.

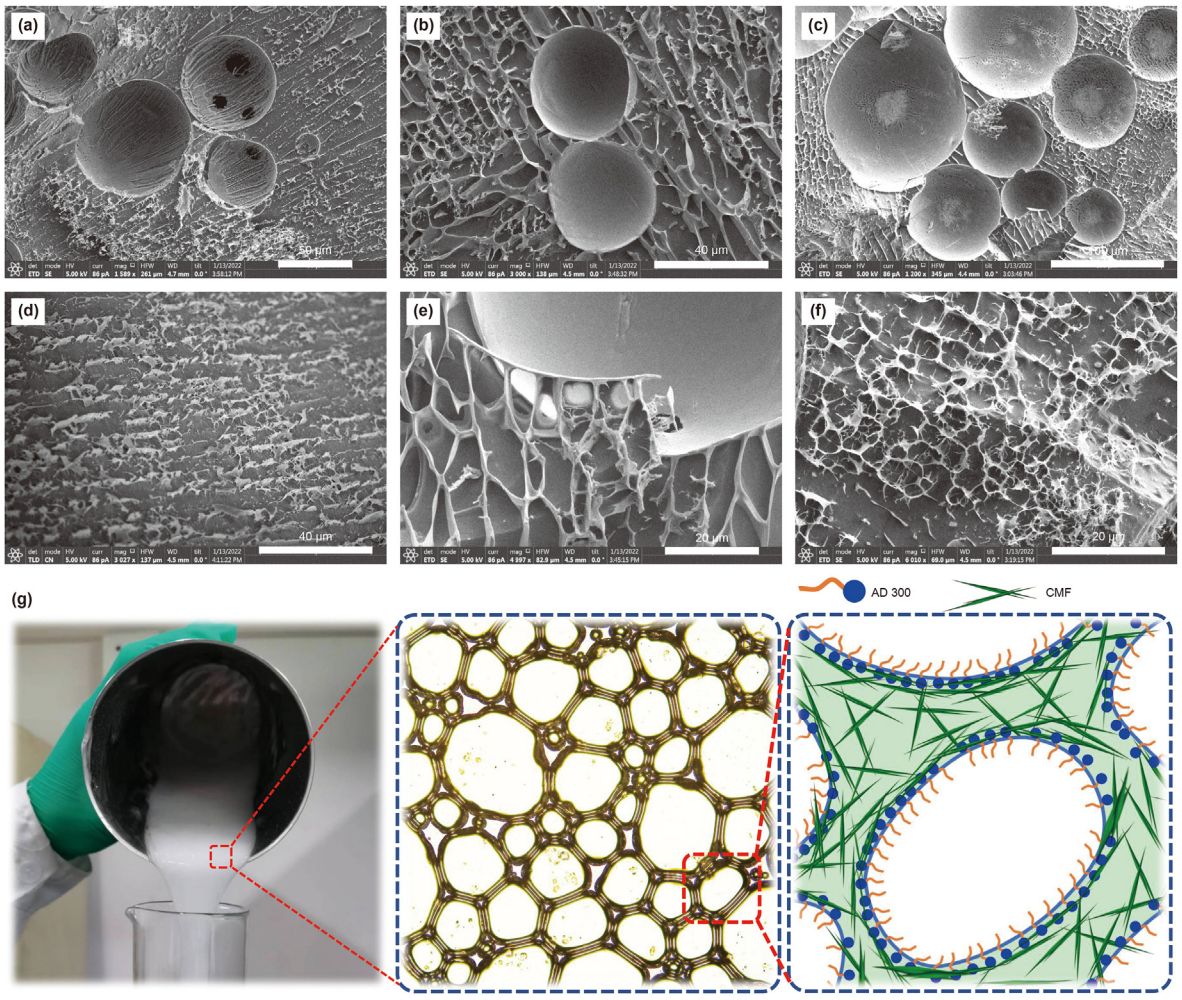

Fig. 7. Micromorphology of the foam stabilized by CMF. (**a**) (**d**) Cryo-SEM images of foam containing CMF only. (**b**) (**e**) Cryo-SEM images of foam containing CMF of 1.0 wt% and NaCl of 6.0 wt%. (**c**) (**f**) Cryo-SEM images of foam containing CMF of 1.0 wt% and $CaCl_2$ of 0.25 wt%. (**g**) Foam stabilizing mechanism of CMF in schematic illustration.

(5) CMF, as a low-cost and environmentally friendly foam stabilizer, is expected to be used under high salinity conditions, especially for oil industry.

Declaration of competing interest

The authors declare that they have no known competing financial interests or personal relationships that could have appeared to influence the work reported in this paper.

Acknowledgements

This work was supported by the National Natural Science Foundation of China (Grant No.51991361 and Grant No.51991362), the foundation of China University of Petroleum (Beijing) (Grant No.2462021YXZZ002).

References

Abascal, D.M., Gracia-Fadrique, J., 2009. Surface tension and foam stability of commercial calcium and sodium caseinates. Food Hydrocolloids 23 (7), 1848–1852. https://doi.org/10.1016/j.foodhyd.2009.02.012.

Alqus, R., Eichhorn, S.J., Bryce, R.A., 2015. Molecular dynamics of cellulose amphiphilicity at the graphene-water interface. Biomacromolecules 16 (6), 1771–1783. https://doi.org/10.1021/acs.biomac.5b00307.

Amani, P., Karakashev, S.I., Grozev, N.A., et al., 2021. Effect of selected monovalent salts on surfactant stabilized foams. Adv. Colloid Interface Sci. 295, 102490. https://doi.org/10.1016/j.cis.2021.102490.

Banerjee, M., Saraswatula, S., Williams, A., et al., 2020. Effect of purification methods on commercially available cellulose nanocrystal properties and TEMPO Oxidation. Processes 8 (6), 698. https://doi.org/10.3390/pr8060698.

Bąkowska, E., Siger, A., Rudzińska, M., et al., 2022. Water content, critical micelle concentration of phospholipids and formation of association colloids as factors influencing autoxidation of rapeseed oil. J. Sci. Food Agric. 102 (2), 488–495. https://doi.org/10.1002/jsfa.11376.

Briceno-Ahumada, Z., Langevin, D., 2017. On the influence of surfactant on the coarsening of aqueous foams. Adv. Colloid Interface Sci. 244, 124–131. https://doi.org/10.1016/j.cis.2015.11.005.

Briscoe, B., Luckham, P., Zhu, S., 2000. The effects of hydrogen bonding upon the viscosity of aqueous poly (vinyl alcohol) solutions. Polymer 41 (10), 3851–3860. https://doi.org/10.1016/S0032-3861(99)00550-9.

Chaiyasit, W., Elias, R.J., McClements, D.J., et al., 2007. Role of physical structures in bulk oils on lipid oxidation. Crit. Rev. Food Sci. Nutr. 47 (3), 299–317. https://doi.org/10.1080/10408390600754248.

Chaturvedi, K.R., Bajpai, S., Trivedi, J., et al., 2022. Air foams for mobility control and subsurface storage of hydrogen in porous media: an experimental study. Energy Fuels 36 (9), 5036–5046. https://doi.org/10.1021/acs.energyfuels.1c04246.

Chaturvedi, K.R., Narukulla, R., Trivedi, J., et al., 2021. Effect of single-step silica nanoparticle on rheological characterization of surfactant based CO_2 foam for effective carbon utilization in subsurface applications. J. Mol. Liq. 341. https://doi.org/10.1016/j.molliq.2021.116905.

Chaturvedi, K.R., Sharma, T., 2021. Rheological analysis and EOR potential of surfactant treated single-step silica nanofluid at high temperature and salinity. J. Petrol. Sci. Eng. 196. https://doi.org/10.1016/j.petrol.2020.107704.

Chen, H., 2014. Chemical composition and structure of natural lignocellulose. Biotechnology of lignocellulose: Theor. Pract. 25–71. https://doi.org/10.1007/978-94-007-6898-7_2.

Conroy, M.W., Taylor, J.C., Farley, J.P., et al., 2013. Liquid drainage from high-expansion (HiEx) aqueous foams during and after filling of a container.

Colloids Surf. A Physicochem. Eng. Asp. 426, 70–97. https://doi.org/10.1016/j.colsurfa.2013.02.050.
Craig, V.S.J., 2004. Bubble coalescence and specific-ion effects. Curr. Opin. Colloid Interface Sci. 9 (1–2), 178–184. https://doi.org/10.1016/j.cocis.2004.06.002.
Czakaj, A., Kannan, A., Wisniewska, A., et al., 2020. Viscoelastic interfaces comprising of cellulose nanocrystals and lauroyl ethyl arginate for enhanced foam stability. Soft Matter 16 (16), 3981–3990. https://doi.org/10.1039/C9SM02392E.
Del Castillo, L.A., Ohnishi, S., Horn, R.G., et al., 2011. Inhibition of bubble coalescence: effects of salt concentration and speed of approach. J. Colloid Interface Sci. 356 (1), 316–324. https://doi.org/10.1016/j.jcis.2010.12.057.
Disalvo, E.A., 1988. Permeability of water and polar solutes in lipid bilayers. Advances in colloid and interface science 1988 29 (1–2), 141–170. https://doi.org/10.1016/0001-8686(88)80004-6.
Emrani, A.S., Nasr-El-Din, H.A., 2017. An experimental study of nanoparticle-polymer-stabilized CO_2 foam. Colloids Surf. A Physicochem. Eng. Asp. 524, 17–27. https://doi.org/10.1016/j.colsurfa.2017.04.023.
Fameau, A.L., Salonen, A., 2014. Effect of particles and aggregated structures on the foam stability and aging. Compt. Rendus Phys. 15 (8–9), 748–760. https://doi.org/10.1016/j.crhy.2014.09.009.
Firouzi, M., Howes, T., Nguyen, A.V., 2015. A quantitative review of the transition salt concentration for inhibiting bubble coalescence. Adv. Colloid Interface Sci. 222, 305–318. https://doi.org/10.1016/j.cis.2014.07.005.
Gupta, S.C., 2019. Promising pathways to lower atmospheric carbon without sacrificing the Petroleum advantage. In: SPE Annual Technical Conference and Exhibition, Calgary. https://doi.org/10.2118/196109-MS.
Ishii, M., Murata, S., Ishitsuka, K., et al., 2022. Stability of novel cellulose-nanofiber-containing foam as environmentally friendly fracturing fluid. J. Petrol. Sci. Eng. 208, 109512. https://doi.org/10.1016/j.petrol.2021.109512.
Joshi, Y.M., 2021. Special topic on dynamics of out of equilibrium soft materials. Phys. Fluids 33 (6), 060401. https://doi.org/10.1063/5.0058356.
Klemm, D., Heublein, B., Fink, H.P., et al., 2005. Cellulose: fascinating biopolymer and sustainable raw material. Angew. Chem. Int. Ed. 44 (22), 3358–3593. https://doi.org/10.1002/anie.200460587.
Liu, L., Borghei, M., Wang, Z., et al., 2018. Salt-induced colloidal destabilization, separation, drying, and redispersion in aqueous phase of cationic and anionic nanochitins. J. Agric. Food Chem. 66 (35), 9189–9198. https://doi.org/10.1021/acs.jafc.8b02062.
Lv, Q., Zhou, T., Luan, Y., et al., 2021. Rheology and dynamic filtration of foam fracturing fluid enhanced by cellulose nanofibrils. In: International Petroleum Technology Conference. Kuala Lumpur. https://doi.org/10.2523/IPTC-21361-MS.
Majeed, T., Kamal, M.S., Solling, T., et al., 2019. Performance evaluation of novel polymers for CO_2 foam enhanced oil recovery. In: Abu Dhabi International Petroleum Exhibition & Conference, Abu Dhabi. https://doi.org/10.2118/197839-MS.
Medronho, B., Romano, A., Miguel, M.G., et al., 2012. Rationalizing cellulose (in) solubility: reviewing basic physicochemical aspects and role of hydrophobic interactions. Cellulose 19 (3), 581–587. https://doi.org/10.1007/s10570-011-9644-6.
Montes Ruiz-Cabello, F.J., Maroni, P., Borkovec, M., 2013. Direct measurements of forces between different charged colloidal particles and their prediction by the theory of Derjaguin, Landau, Verwey, and Overbeek (DLVO). J. Chem. Phys. 138 (23), 234705. https://doi.org/10.1063/1.4810901.
Murray, B.S., Dickinson, E., Gransard, C., et al., 2006. Effect of thickeners on the coalescence of protein-stabilized air bubbles undergoing a pressure drop. Food Hydrocolloids 20 (1), 114–123. https://doi.org/10.1016/j.foodhyd.2005.03.010.
Narukulla, R., Chaturvedi, K.R., Ojha, U., et al., 2022. Carbon dioxide capturing evaluation of polyacryloyl hydrazide solutions via rheological analysis for carbon utilization applications. Energy 241, 122929. https://doi.org/10.1016/j.energy.2021.122929.
Novev, J.K., Panchev, N., Slavchov, R.I., 2017. Evaporating foam films of pure liquid stabilized via the thermal Marangoni effect. Chem. Eng. Sci. 171, 520–533. https://doi.org/10.1016/j.ces.2017.06.016.
Pandey, A., Sinha, A.S.K., Chaturvedi, K.R., et al., 2021. Experimental investigation on effect of reservoir conditions on stability and rheology of carbon dioxide foams of nonionic surfactant and polymer: implications of carbon geo-storage. Energy 235. https://doi.org/10.1016/j.energy.2021.121445.
Pu, W.F., Wei, P., Sun, L., et al., 2017. Experimental investigation of viscoelastic polymers for stabilizing foam. J. Ind. Eng. Chem. 47, 360–367. https://doi.org/10.1016/j.jiec.2016.12.006.
Qiao, X., Miller, R., Schneck, E., et al., 2020. Influence of pH on the surface and foaming properties of aqueous silk fibroin solutions. Soft Matter 16 (15), 3695–3704. https://doi.org/10.1039/C9SM02372K.
Rio, E., Biance, A.L., 2014. Thermodynamic and mechanical timescales involved in foam film rupture and liquid foam coalescence. ChemPhysChem 15 (17), 3692–3707. https://doi.org/10.1002/cphc.201402195.
Said, M.S., Jaafar, M.Z., Omar, S., et al., 2022. Influence of whey protein isolate on CO_2 foams stability in three different types of crude oil. Case Studies in Chemical and Environmental Engineering 5, 100191. https://doi.org/10.1016/j.cscee.2022.100191.
Sharma, T., Joshi, A., Jain, A., et al., 2022. Enhanced oil recovery and CO_2 sequestration potential of Bi-polymer polyvinylpyrrolidone-polyvinyl alcohol. J. Petrol. Sci. Eng. 211, 110167. https://doi.org/10.1016/j.petrol.2022.110167.
Singh, A., Chaturvedi, K.R., Sharma, T., 2021. Natural surfactant for sustainable carbon utilization in cleaner production of fossil fuels: extraction, characterization and application studies. J. Environ. Chem. Eng. 9 (5), 106231. https://doi.org/10.1016/j.jece.2021.106231.
Sun, L., Bai, B., Wei, B., et al., 2019. Recent advances of surfactant-stabilized N_2/CO_2 foams in enhanced oil recovery. Fuel 241, 83–93. https://doi.org/10.1016/j.fuel.2018.12.016.
Tang, Q., Huang, Z., Wang, B., et al., 2020. Surfactant-free aqueous foams stabilized with synergy of xanthan-based amphiphilic biopolymer and nanoparticle as potential hydraulic fracturing fluids. Colloids Surf. A Physicochem. Eng. Asp. 603, 125215. https://doi.org/10.1016/j.colsurfa.2020.125215.
Viturawong, Y., Achayuthakan, P., Suphantharika, M., 2008. Gelatinization and rheological properties of rice starch/xanthan mixtures: effects of molecular weight of xanthan and different salts. Food Chem. 111 (1), 106–114. https://doi.org/10.1016/j.foodchem.2008.03.041.
Wang, D., Hou, Q., Luo, Y., et al., 2013. Stability comparison between particles-stabilized foams and polymer-stabilized foams. J. Dispersion Sci. Technol. 36 (2), 268–273. https://doi.org/10.1080/01932691.2013.859625.
Wang, F., Li, Z., Chen, H., et al., 2017. Establishment and application of a structure evolution model for aqueous foam based on fractal theory. RSC Adv. 7 (7), 3650–3659. https://doi.org/10.1039/C6RA24790C.
Wang, H., Wei, X., Du, Y., et al., 2019. Experimental investigation on the dilatational interfacial rheology of dust-suppressing foam and its effect on foam performance. Process Saf. Environ. Protect. 123, 351–357. https://doi.org/10.1016/j.psep.2019.01.027.
Wang, T., Yang, L., Jiang, G., et al., 2020. Enhanced foam-stabilizing performance by the addition of clays: a comparison of magnesium aluminum silicate with sodium bentonite. Appl. Clay Sci. 189, 105558. https://doi.org/10.1016/j.clay.2020.105558.
Wang, Z., Elimelech, M., Lin, S., 2016. Environmental applications of interfacial materials with special wettability. Environ. Sci. Technol. 50 (5), 2132–2150. https://doi.org/10.1021/acs.est.5b04351.
Wei, P., Zhai, K., Guo, K., et al., 2022. Highly viscous liquid foam for oil-displacement: surface & phase behavior enhancement. J. Petrol. Sci. Eng. 212, 110274. https://doi.org/10.1016/j.petrol.2022.110274.
Xiang, W., Preisig, N., Ketola, A., et al., 2019. How cellulose nanofibrils affect bulk, surface, and foam properties of anionic surfactant solutions. Biomacromolecules 20 (12), 4361–4369. https://doi.org/10.1021/acs.biomac.9b01037.
Xiao, M., Frey, M.W., 2008. Rheological studies of the interactions in cellulose/ethylene diamine/salt systems. J. Polym. Sci. B Polym. Phys. 46 (21), 2326–2334. https://doi.org/10.1002/polb.21564.
Xie, G., Huang, D.C., Deng, M.Y., et al., 2019. Investigating the role of alkyl chain length of the inhibitors on its intercalation inhibiting mechanism in sodium montmorillonite. Energy Fuels 33 (6), 5182–5190. https://doi.org/10.1021/acs.energyfuels.9b00969.
Yaminsky, V.V., Ohnishi, S., Vogler, E.A., et al., 2010. Stability of aqueous films between bubbles. Part 1. The effect of speed on bubble coalescence in purified water and simple electrolyte solutions. Langmuir 26 (11), 8061–8074. https://doi.org/10.1021/la904481d.
Yang, L., Wang, T., Yang, X., et al., 2019. Highly stabilized foam by adding amphiphilic janus particles for drilling a high-temperature and high-calcium geothermal well. Ind. Eng. Chem. Res. 58 (23), 9795–9805. https://doi.org/10.1021/acs.iecr.9b01714.
Yao, X., Yi, P., Zhao, G., et al., 2018. A study of the stability mechanism of the dispersed particle gel three-phase foam using the interfacial dilational rheology method. Materials 11 (5), 699. https://doi.org/10.3390/ma11050699.
Yokota, S., Tagawa, S., Kondo, T., 2021. Facile surface modification of amphiphilic cellulose nanofibrils prepared by aqueous counter collision. Carbohydrate Polym. 255, 117342. https://doi.org/10.1016/j.carbpol.2020.117342.
Zhang, L., Tian, L., Du, H., et al., 2017. Foams stabilized by surfactant precipitates: criteria for ultrastability. Langmuir 33 (29), 7305–7311. https://doi.org/10.1021/acs.langmuir.7b01962.
Zhu, Y., Tian, J., Hou, Q., et al., 2017. Studies on nanoparticle-stabilized foam flooding EOR for a high temperature and high salinity reservoir. In: Abu Dhabi International Petroleum Exhibition & Conference, Abu Dhabi. https://doi.org/10.2118/188964-MS.